

---

---

# Tumor-Absorbed Dose Predicts Progression-Free Survival Following $^{131}\text{I}$ -Tositumomab Radioimmunotherapy

Yuni K. Dewaraja<sup>1</sup>, Matthew J. Schipper<sup>2</sup>, Jincheng Shen<sup>3</sup>, Lauren B. Smith<sup>4</sup>, Jure Murgic<sup>5</sup>, Hatice Savas<sup>1</sup>, Ehab Youssef<sup>1</sup>, Denise Regan<sup>1</sup>, Scott J. Wilderman<sup>6</sup>, Peter L. Roberson<sup>2</sup>, Mark S. Kaminski<sup>7</sup>, and Anca M. Avram<sup>1</sup>

<sup>1</sup>Department of Radiology, University of Michigan, Ann Arbor, Michigan; <sup>2</sup>Department of Radiation Oncology, University of Michigan, Ann Arbor, Michigan; <sup>3</sup>Department of Biostatistics, University of Michigan, Ann Arbor, Michigan; <sup>4</sup>Department of Pathology, University of Michigan, Ann Arbor, Michigan; <sup>5</sup>Department of Oncology and Nuclear Medicine, University Hospital Center Sestre Milosrdnice, Zagreb, Croatia; <sup>6</sup>Department of Nuclear Engineering, University of Michigan, Ann Arbor, Michigan; and <sup>7</sup>Department of Internal Medicine, University of Michigan, Ann Arbor, Michigan

The study aimed at identifying patient-specific dosimetric and nondosimetric factors predicting outcome of non-Hodgkin lymphoma patients after  $^{131}\text{I}$ -tositumomab radioimmunotherapy for potential use in treatment planning. **Methods:** Tumor-absorbed dose measures were estimated for 130 tumors in 39 relapsed or refractory non-Hodgkin lymphoma patients by coupling SPECT/CT imaging with the Dose Planning Method (DPM) Monte Carlo code. Equivalent biologic effect was calculated to assess the biologic effects of nonuniform absorbed dose including the effects of the unlabeled antibody. Evaluated nondosimetric covariates included histology, presence of bulky disease, and prior treatment history. Tumor level outcome was based on volume shrinkage assessed on follow-up CT. Patient level outcome measures were overall response (OR), complete response (CR), and progression-free survival (PFS), determined from clinical assessments that included PET/CT. **Results:** The estimated mean tumor-absorbed dose had a median value of 275 cGy (range, 94–711 cGy). A high correlation was observed between tracer-predicted and therapy-delivered mean tumor-absorbed doses ( $P < 0.001$ ;  $r = 0.85$ ). In univariate tumor-level analysis, tumor shrinkage correlated significantly with almost all of the evaluated dosimetric factors, including equivalent biologic effect. Regression analysis showed that OR, CR, and PFS were associated with the dosimetric factors and equivalent biologic effect. Both mean tumor-absorbed dose ( $P = 0.025$ ) and equivalent biologic effect ( $P = 0.035$ ) were significant predictors of PFS whereas none of the nondosimetric covariates were found to be statistically significant factors affecting PFS. The most important finding of the study was that in Kaplan–Meier curves stratified by mean dose, longer PFS was observed in patients receiving mean tumor-absorbed doses greater than 200 cGy than in those receiving 200 cGy or less (median PFS, 13.6 vs. 1.9 mo for the 2 dose groups; log-rank  $P < 0.0001$ ). **Conclusion:** A higher mean tumor-absorbed dose was significantly predictive of improved PFS after  $^{131}\text{I}$ -tositumomab radioimmunotherapy. Hence tumor-absorbed dose, which can be estimated before therapy, can potentially be used to design radioimmunotherapy protocols to improve efficacy.

**Key Words:** dosimetry; radioimmunotherapy; progression free survival; SPECT/CT; non-Hodgkin lymphoma

**J Nucl Med 2014; 55:1047–1053**

DOI: 10.2967/jnumed.113.136044

**M**ost advanced low-grade non-Hodgkin lymphoma (NHL) patients who undergo conventional treatment, such as chemotherapy and external radiotherapy, eventually relapse and die of their disease. Therapy with radiolabeled monoclonal antibodies, such as  $^{131}\text{I}$ -tositumomab and  $^{90}\text{Y}$ -ibritumomab tiuxetan, has offered new therapeutic options for such patients, with reported overall response (OR) rates in the 60%–83% range in previously treated patients (1) and 95% in frontline patients (2). Currently, the protocol for determining the amount of therapeutic radioactivity to administer to each patient is based on patient weight in the case of  $^{90}\text{Y}$ -ibritumomab tiuxetan and based on delivering 75 cGy to the whole body in the case of  $^{131}\text{I}$ -tositumomab. Instead of this conservative approach, a more aggressive dosimetry-driven approach would be to tailor the treatment to deliver an optimal therapeutic dose to the tumor while avoiding critical organ toxicity. Because of the radio-sensitivity of NHL, even modest dose escalation can potentially lead to considerably improved response (3).

To adopt a precision-medicine approach to radioimmunotherapy, accurate and highly patient-specific methods must be used for tumor and normal organ dose estimation. Conventional dose estimation methods rely on 2-dimensional planar imaging and model-based approximations of the human anatomy to calculate a mean absorbed dose to a generic target. In radioimmunotherapy, however, the distribution of radiolabeled antibodies in tumor is heterogeneous, leading to nonuniform dose distributions, which can affect response. Recent studies evaluating tumor dose–response have used 3-dimensional (3D) imaging and highly accurate and patient-specific dosimetry methods such as Monte Carlo simulation. To date, however, such studies have failed to show a statistically significant relationship between dose and effect in radioimmunotherapy of NHL, even when 3D dosimetric parameters (such as minimum dose to any part of the tumor, for example) were used instead of mean dose (4,5). However, an improved dose–response correlation was demonstrated with 3D dosimetry incorporating radiobiologic modeling, including effects of the unlabeled antibody (5).

Received Dec. 11, 2013; revision accepted Mar. 21, 2014.

For correspondence or reprints contact: Yuni K. Dewaraja, Department of Radiology, University of Michigan, 1301 Catherine, 2276 Medical Science I/5610, Ann Arbor, MI 48109.

E-mail: yuni@umich.edu

Published online May 19, 2014.

COPYRIGHT © 2014 by the Society of Nuclear Medicine and Molecular Imaging, Inc.

In past studies investigating dose–response in radioimmunotherapy of NHL, response was assessed as the reduction in tumor size or as the clinical response classification at follow-up at around 2–6 mo (4–6). In the present study, in addition to these previously used efficacy measures, we focus on progression-free survival (PFS), which is growing in prevalence as the primary endpoint in oncology studies. Here, the associations between these outcome measures and dosimetric measures determined by coupling SPECT/CT imaging with Monte Carlo–based 3D dosimetry were evaluated. In addition, recognizing that dose-related factors alone will have limited ability to predict the outcome of radioimmunotherapy, we also evaluated dosimetric measures that incorporate radiobiology as well as non-dosimetric prognostic factors, such as histology and prior treatment history. Most of the factors evaluated, including the tumor-absorbed dose, can be estimated before therapy. Hence, establishing the association between these factors and outcome can potentially lead to better patient selection or selected dose escalation to improve efficacy in future radioimmunotherapy protocols.

## MATERIALS AND METHODS

### Patients

The study enrolled 39 relapsed or refractory NHL patients being treated with  $^{131}\text{I}$ -tositumomab at the University of Michigan between November 2005 and August 2012, who volunteered for research SPECT/CT imaging. This group included 32 patients conventionally treated with  $^{131}\text{I}$ -tositumomab and 7 patients treated as part of a phase I clinical trial of radiosensitization using bortezomib (Velcade; Millennium Pharmaceuticals, Inc.) along with  $^{131}\text{I}$ -tositumomab. For the present research, the treatment protocol was unchanged, but patients gave separate informed consent for SPECT/CT imaging, which received approval by the University of Michigan Internal Review Board.

### Treatment

The radiolabeled antibody administration, which includes injection of 450 mg of the unlabeled tositumomab before both the tracer and the therapeutic administration of  $^{131}\text{I}$ -tositumomab, has been described previously (2). From planar  $\gamma$  camera whole-body measurements after the tracer (185 MBq) administration, the amount of radioactivity necessary to deliver 75 cGy (65 cGy if platelet count is  $< 150,000/\mu\text{L}$ ) to the whole body is determined for each patient and is then administered roughly 8 d later. The administered therapy activity for the 39 patients ranged from 2.2 to 5.7 GBq, with a median value of 3.1 GBq.

### Imaging, Activity Quantification, and Dosimetry

SPECT/CT imaging on a Siemens Symbia system was performed after the tracer (on days 0, 2, and 6) and therapy (on days 2, 5, and 7–9) administration. Posttracer imaging was used to calculate the absorbed dose delivered by the tracer, which was then scaled by the ratio of therapy–to–tracer administered activity to determine a tracer-predicted absorbed dose. Posttherapy imaging was used to determine the therapy-delivered absorbed dose.

The SPECT activity quantification has been described previously (5) and included in-house–developed 3D ordered-subset expectation maximization reconstruction with correction for image-degrading physical factors. Tumor outlines defined on the CT portion of each of the 6 scans by a radiologist were applied to coregistered SPECT images (Fig. 1), and target counts were converted to activity using a calibration factor and recovery coefficients (RCs) determined from phantom measurements with hot spheres. Tumor and the rest-of-the-body time–activity data were fitted with bi- and monoexponential functions, respectively.

SPECT activity maps and CT-defined density maps at each time point were input to the Dose Planning Method (DPM) Monte Carlo

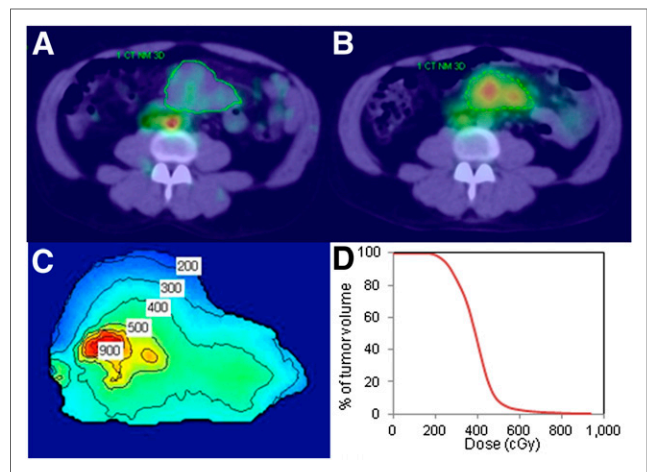


**FIGURE 1.** Imaging and dosimetry. Day 0 posttracer (A) and day 2 posttherapy (B) SPECT/CT images of patient with CT-defined tumor outlines. Tumor-absorbed dose distribution with isodose contours in cGy (C) and tumor dose–volume histogram (D).

code (7) to determine the dose–rate maps, which were multiplied by activity as a function of time and integrated to obtain 3D dose distributions, as described previously (5). This calculation included deformable image registration to account for tumor voxels that change over time because of deformation or regression. The voxel-level calculation allowed for estimation of not only mean tumor-absorbed dose but also other measures such as minimum dose and D99 (or D80), which is defined here as the absorbed dose received or exceeded by 99% (or 80%) of the tumor volume. These measures can be meaningful when there is significant nonuniformity in the tumor uptake (Fig. 1). In addition, for each tumor the equivalent biologic effect was calculated to assess the biologic effects of the nonuniform absorbed dose (8), including the variable effects of the unlabeled antibody (cold effect), tumor radiosensitivity ( $\alpha$ ), and effects of cell proliferation, as described previously (9). Radiation sensitivity, cold effect, and proliferation parameters were estimated on the basis of biologic effect and cell clearance model fits to changes in tumor volumes measured on SPECT/CT. Equivalent biologic effect (E), the negative log of the cumulative clonogenic cell surviving fraction, was used here instead of the more familiar equivalent uniform dose ( $\text{EUD} = E/\alpha$ ). EUD may have diminished usefulness as the relevant patient outcome score for biologic modeling because of the variability of nondose quantities in the isoeffect equation (i.e., cold effect, radiosensitivity, and proliferation) for this patient population.

The tracer imaging data were used only in predicting the mean tumor-absorbed dose and not the other 3D parameters such as minimum dose. Although the 3D dosimetric measures can be predicted from the tracer study, when counting rates are low these voxel-level estimates can be noisy. Methodologies to improve the accuracy of noisy SPECT images, such as postreconstruction filtering (10), were not used here.

### Assessment of Tumor Shrinkage and Efficacy

All patients had a first follow-up at around 2 mo (6–10 wk) after treatment, and all but 3 had a second at around 6 mo after treatment. Subsequently, the patients were seen about every 6 mo. Follow-ups typically included  $^{18}\text{F}$ -FDG PET/CT imaging or CT imaging.

Only the first follow-up CT was used in assessing tumor-level volume shrinkage because most patients who did not have a complete response (CR) at this point (15/22 such cases) went on to receive alternative therapies (such as external radiation) after the first follow-up. Tumor volumes were defined by a radiologist on the CT portion of the first follow-up PET/CT or CT (Fig. 2B) and compared with the

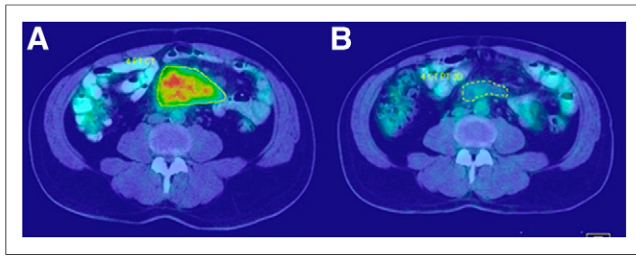


**FIGURE 2.** Baseline (A) and follow-up (B) PET/CT scans used to assess response after radioimmunotherapy (same patient as in Fig. 1).

baseline volumes defined on the first SPECT/CT (Fig. 1A) to calculate shrinkage.

For patient-level response, classification in clinical follow-up records, which is based on both CT and PET assessment (11), was used. For OR, CR and partial response (PR) cases were grouped as responders (OR = 1), and progressive disease and stable disease cases were grouped as nonresponders (OR = 0). Any patient who had additional therapy (chemotherapy or radiation therapy) before the first follow-up imaging was considered a nonresponder. PFS was defined as the minimum time to progression, relapse, or death from any cause and was calculated from the date of the tracer administration. Patients alive and without evidence of progression were censored at the last date at which they were assessed.

### Statistical Analysis

In tumor-level analyses, the Pearson correlation coefficient was calculated to quantify the correlation between predicted and delivered mean tumor-absorbed doses. Rank-based (Spearman) correlation coefficients were computed to quantify the correlation between tumor volume shrinkage and the covariates evaluated at the tumor level. Here, Spearman correlations were used rather than Pearson because some of these relationships were nonlinear. Null hypotheses of no correlation (i.e.,  $r = 0$ ) were tested.

In the models for patient-level outcome, patient-level dose values and equivalent biologic effect were calculated as the average of tumor-level summaries. Logistic regression models were used to assess the relation between response (OR, CR) and various dose and other patient-level covariates. Cox proportional hazards regression models were used to assess the relation between PFS times and dose and other covariates. The Kaplan–Meier method was used to summarize PFS times for all patients and for various dose-defined groups. The log-rank test was used to compare PFS between dose groups.

To account for possible confounding of results due to heterogeneity of the histology (indolent vs. transformed) or treatment (with or without the radiosensitizer), sensitivity analyses were performed by repeating all analyses after excluding patients with a transformed histology ( $n = 8$ ) and separately excluding patients who received the radiosensitizer ( $n = 7$ ). Results of these analyses were similar to analysis of the complete dataset and hence are not presented here. Because of the small number of patients, it was not possible to separately study these groups. In all analyses, 2-sided  $P$  values of less than 0.05 were considered statistically significant. The SAS system (version 9.3; SAS Institute) was used for all analysis.

## RESULTS

The baseline disease and patient characteristics examined here are summarized in Table 1.

### Tumor Shrinkage and Efficacy

All tumors within the SPECT/CT field of view that were greater than 1 mL and well differentiated on CT were outlined (a total of

130 tumors). In general, tumors were large, with a median baseline volume of 20 mL (range, 1–716 mL). The number of individual tumors outlined in each patient had a median value of 2 (range, 1–9). To evaluate effects of the unlabeled antibody, the change in tumor volume over the 6 d of tracer imaging (before therapy administration) was assessed and found to have a median value of 10.2% (range, –48% to 47%).

It was not possible to determine the tumor shrinkage at first follow-up for 6 patients, 4 of them due to difficulty obtaining scans from outside institutions and 2 of them because the patients underwent external radiation therapy before the first follow-up scan. For the remaining 33 patients, the median tumor shrinkage was 81% (range, –155% to 100%).

Twenty-four of the 39 (62%) patients were classified as responders, with 18 (46%) classified as complete responders. The median follow-up time for patients who did not progress, relapse, or die was 14.8 mo (range, 1.9–52.4 mo). Three patients for whom follow-up information was not available after the first visit were censored at that time. At the time of analysis, 9 of the 37 patients in follow-up were in remission, 19 patients had relapsed, and 9 had died. Overall, the median PFS time was 6.6 mo (95% confidence interval, 2.8–15.2 mo).

### Dose-Related Factors

The median (over all patients) value of the tracer-predicted mean tumor-absorbed dose was 248 cGy (range, 80–768 cGy) and that of the therapy-delivered mean tumor-absorbed dose was 275

**TABLE 1**  
Patient and Disease Characteristics at Time of  
Radioimmunotherapy ( $n = 39$ )

Characteristic	$n$ or value
Age (y)	
Median	54
Range	33–81
Male sex	29 (74)
Histology	
Indolent*	31 (79)
Transformed (diffuse large B cell)	8 (21)
Stage of disease†	
I	4 (11)
II	14 (37)
III	11 (29)
IV	9 (24)
Chemotherapy‡ refractory	22 (56)
No. of prior chemotherapy regimens	
Median	1
Range	1–5
Bone marrow involvement†	
0%	26 (68)
1%–25%	12 (32)
No. of tumor sites	
Median	3
Range	1–7
Presence of bulky disease§	10 (26)
High lactate dehydrogenase	12 (31)

\*30 follicular, 1 marginal zone. Of the patients with follicular lymphoma, 26 were grade 1 or 2 and 4 were grade 3.

†1 unknown.

‡Chemotherapy or rituximab.

§At least 1 tumor with diameter more than 7 cm.

Data in parentheses are percentages.

cGy (range, 94–711 cGy). These results and 3D dosimetric measures are summarized in Table 2.

### Correlation and Regression Analyses

**Tumor-Level Analysis.** The correlation between tumor shrinkage and the covariates evaluated at the tumor level are summarized in Table 2. A statistically significant positive correlation was observed between tumor shrinkage and all of the dose-related factors evaluated except for the minimum dose. The correlation between tumor shrinkage and baseline tumor volume or between tumor shrinkage and initial shrinkage during tracer imaging was not statistically significant.

Additionally, the relationship between predicted and delivered tumor-absorbed dose was assessed and found to be strongly correlated ( $P < 0.001$ ;  $r = 0.855$ ). The correlation between mean tumor-absorbed dose and baseline tumor volume was also assessed but was found to be not significant.

**Patient-Level Analysis.** Summaries of the patient-level regression analysis are given in Table 3. With only a single exception (presence of bulky disease and OR), the nondose factors were not found to be predictive of patient outcome. In contrast, the mean tumor-absorbed dose and equivalent biologic effect show an association with all 3 outcome measures. Both the predicted ( $P = 0.02$ ) and the delivered ( $P = 0.025$ ) mean tumor-absorbed doses and equivalent biologic effect ( $P = 0.035$ ) were significant predictors of PFS. In Table 3, odds ratios and hazard ratios (HRs) are reported for a 50-cGy change in absorbed dose. Here an HR greater than 1 implies that the hazard of progression increases (or time to progression decreases) as the variable increases, whereas an HR less than 1 implies that the hazard decreases (or time to progression increases) as the variable increases. For example, the HR for therapy-delivered mean tumor dose is 0.75, implying a 25% reduction in the hazard of progression for each 50-cGy increase in absorbed dose.

Because of the clinical significance of this result, the relation between mean tumor-absorbed dose and PFS was further analyzed by splitting patients into 10 approximately equal-size groups based on their dose values and calculating the hazard for each group relative to the hazard for the highest-dose group (Fig. 3). Such analysis permits the determination of whether the relation between dose and hazard of progression is linear or otherwise. Although there is substantial noise in this plot due to the small

number of patients (3–5 in each group), it clearly shows decreasing hazards when going from 0 to 200 cGy. Beyond 200 cGy, the change in hazard is relatively small. Hence, a threshold of 200 cGy was used for stratification of Kaplan–Meier curves into 2 patient groups of high and low mean tumor-absorbed doses (of the 39 patients, 30 patients received a mean tumor-absorbed dose  $> 200$  cGy). As illustrated in Figure 4, significantly longer PFS times were observed in patients whose mean tumor-absorbed dose was greater than 200 cGy than in those receiving 200 cGy or less. Overall for all patients, the median PFS was 6.6 mo, whereas for the 2 dose groups analyzed separately the median PFS was 13.6 mo (95% confidence interval, 5.7–26.5 mo) versus 1.9 mo (95% confidence interval, 1.0–3.4 mo) (log-rank  $P < 0.0001$ ). Twenty-three of the 30 patients in the higher-dose group were responders (OR rate of 77%), whereas only 1 of the 9 patients in the lower-dose group responded (OR rate of 11%).

### DISCUSSION

Although evaluating efficacy was not the focus of the present work, response rates and PFS observed here agreed well with previously published data for this patient cohort. The OR rate of 62% and CR rate of 46% in the present study compare well with the OR rate of 56% and CR rate of 30% reported in an integrated efficacy analysis of 250 patients in 5 clinical trials of  $^{131}\text{I}$ -tositumomab radioimmunotherapy in NHL (12). Similarly, the overall median PFS of 6.6 mo compares favorably with the overall median PFS of 6.4 mo reported in the previous efficacy study.

The mean tumor-absorbed dose values of the present study (median, 275 cGy; range, 94–711 cGy) are consistent with a previous study that reported a median tumor-absorbed dose of 300 cGy (range, 37–1760 cGy) with SPECT-based dosimetry for a similar patient cohort (4). The current study used sophisticated patient-specific methods for imaging and dose estimation. However, because of the poor spatial resolution of  $^{131}\text{I}$  SPECT there can be significant inaccuracies associated with activity quantification in tumors with dimensions that are small, compared with the system resolution, or have irregular shapes relative to the spheric shape used to determine RCs. In general though, the lymphoma tumors examined here were relatively large (median value, 20 mL), and highly irregular shapes were not typical.

**TABLE 2**

Univariate Analysis of Relationship Between Tumor Shrinkage at 2 Months and Covariates Evaluated at Tumor Level

Parameter	Median	n	Correlation with tumor volume shrinkage	
			P	r*
Baseline tumor volume (mL)	20 (1–716)	130	0.078	–0.166
Initial shrinkage (during tracer imaging) (%)	10 (–48 to 47)	130	0.163	0.132
Tracer-predicted mean tumor-absorbed dose (cGy)	248 (80–768)	130	0.002	0.290
Therapy-delivered mean tumor-absorbed dose (cGy)	275 (94–711)	124	0.021	0.222
Therapy-delivered minimum tumor dose (cGy)	130 (2–382)	124	0.078	0.171
Therapy-delivered tumor D99 (cGy)	156 (29–408)	124	0.034	0.204
Therapy-delivered tumor D80 (cGy)	216 (58–481)	124	0.021	0.222
Therapy-delivered equivalent biologic effect	0.87 (0.004–6.57)	124	$<0.0001$	0.490

\*Spearman rank correlation was used.

D99 and D80 = absorbed dose received or exceeded by 99% and 80%, respectively.

Data in parentheses are ranges.

**TABLE 3**  
Univariate Analysis of Relationship Between Patient Level Outcome Measures and Covariates

Parameter	Outcome					
	OR		CR		PFS	
	Odds ratio*	P	Odds ratio*	P	HR*	P
Sex (M vs. F)	0.607	0.526	0.813	0.777	1.311	0.532
Age (y)	0.998	0.431	0.973	0.327	1.015	0.348
Stage (III/IV vs. I/II)	2.333	0.211	1.571	0.493	0.775	0.513
Histology (transformed vs. indolent)	0.550	0.455	0.640	0.584	1.492	0.362
Presence of bulky disease (Y vs. N)	0.163	0.024	0.400	0.242	1.604	0.291
Number of tumor sites	1.365	0.122	1.199	0.305	0.976	0.808
Marrow involvement (Y vs. N)	4.285	0.094	1.909	0.361	1.131	0.762
Elevated lactate dehydrogenase (Y vs. N)	0.824	0.784	1.250	0.748	1.488	0.313
Chemotherapy refractory (Y vs. N)	0.500	0.310	0.400	0.167	1.401	0.397
No. of prior chemotherapies	0.612	0.137	0.569	0.131	1.257	0.193
Tracer-predicted tumor-absorbed dose (cGy) <sup>†</sup>	1.468	0.061	1.535	0.032	0.773	0.020
Therapy-delivered tumor-absorbed dose (cGy) <sup>†</sup>	1.455	0.060	1.331	0.100	0.750	0.025
Therapy-delivered tumor equivalent biologic effect <sup>†</sup>	1.557	0.011	1.306	0.022	0.894	0.035

\*Odds ratio and HR calculated for 50-cGy change in absorbed dose, 0.15-unit change in equivalent biologic effect, and 1-unit change in other continuous factors.

<sup>†</sup>Averaged over multiple tumors in each patient.

The robust correlation shown here between tracer-predicted and therapy-delivered mean tumor-absorbed doses (with  $n = 124$ ) is of much significance for treatment planning and has been demonstrated previously for a smaller sample size (13). The correlation between 2-mo tumor shrinkage and the initial tumor shrinkage during tracer imaging was also evaluated because this quantity can be determined before therapy, but the correlation was not significant. The pretherapy shrinkage can be attributed to the unlabeled antibody, which has been shown to have some therapeutic effect (14). As has been reported previously for a similar cohort (4), the baseline tumor size did not correlate with tumor shrinkage or the tumor-absorbed dose in a statistically significant manner, indicating that the antibody uptake per gram of tumor is fairly constant.

At the tumor level, although a statistically significant correlation was demonstrated between most of the dosimetric parameters and tumor shrinkage at around 2 mo, there was high scatter in these data, as evidenced by the low  $r$  values (Table 2). No advantage was found in using 3D dosimetric parameters, compared with using mean tumor-absorbed dose, but the correlation improved when 3D dosimetry was combined with radiobiologic modeling (higher  $r$  and lower  $P$  for equivalent biologic effect in Table 2). Similarly in the patient-level logistic regression, the  $P$  values were smaller when equivalent biologic effect was used instead of mean tumor-absorbed dose (Table 3). Past studies have also failed to show improvement in dose-response by merely using measures from 3D dosimetry without the introduction of radiobiologic modeling (4,5). This is likely because the loss of effectiveness due to dose nonuniformity alone is not substantial at the low absorbed doses and dose-rates encountered in this type of therapy, as shown previously (5). In addition, when SPECT is used to determine voxel-level nonuniformities, inaccuracies can be significant because of the poor spatial resolution (15). Although RCs were used here to correct for resolution effects when quantifying total tumor activity, this was not a voxel-level correction.

Both mean tumor-absorbed dose and equivalent biologic effect showed similar statistically significant association with PFS (Table 3).

Thus, in terms of the long-term predictive ability there does not appear to be an advantage in using our current implementation of equivalent biologic effect over using the mean tumor-absorbed dose. In addition, tumor-absorbed doses can be estimated before therapy, whereas equivalent biologic effect cannot be determined before therapy because the radiosensitivity and cold-antibody sensitivity parameters required for the calculation can, at present, be computed only when both posttracer and posttherapy imaging data are available (9). Variations in model fit parameters used to calculate equivalent biologic effect here were extreme (e.g., 0.05–2.0 Gy<sup>-1</sup> for  $\alpha$ ), implying that the potential to calculate equivalent biologic effect before therapy depends on correlating model parameters with independent information. Initial efforts have explored correlations with biomarkers of proliferation (Ki-67) and radiosensitivity (p53) (16).

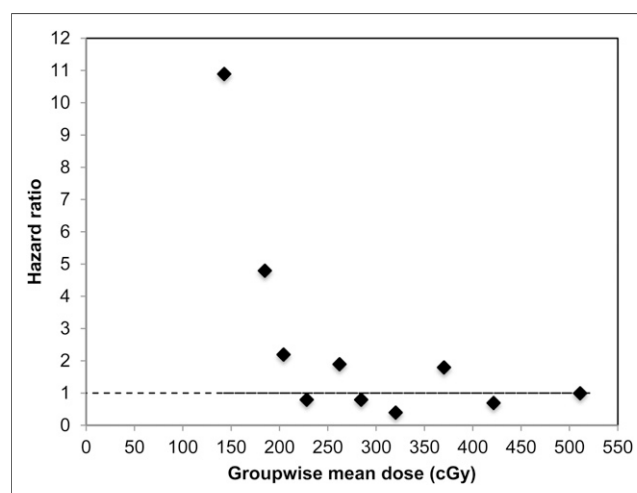


**FIGURE 3.** Estimated relative HR for each decile-defined group based on mean tumor dose. HR here was calculated relative to HR for highest-dose decile group.

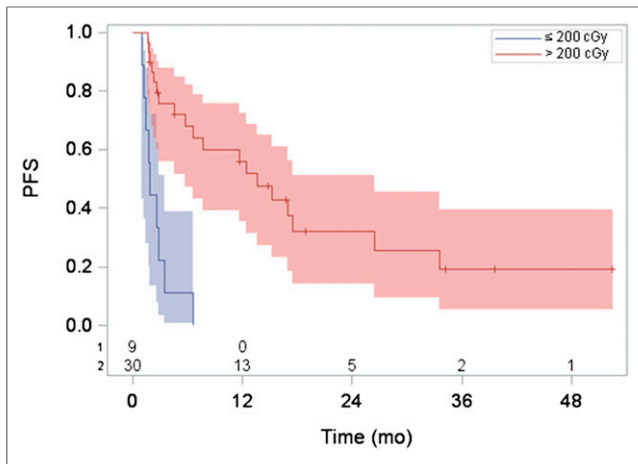


**FIGURE 4.** PFS (with number of subjects at risk and 95% confidence limits indicated) stratified by mean tumor-absorbed dose  $> 200$  cGy and  $\leq 200$  cGy. Median PFS was 13.6 vs. 1.9 mo for the 2 dose groups (log-rank  $P < 0.0001$ ).

None of the nondosimetric covariates evaluated were found to be statistically significant factors affecting outcome except for the association between bulky disease and OR. This finding is possibly because of the relatively small sample size, which is a limitation of our study. Thus, the clinical relevance of these results needs to be determined with higher numbers. Some of the factors evaluated, such as histology, lactate dehydrogenase, and bulky disease, have been shown to be significantly predictive of response to  $^{131}\text{I}$ -tositumomab radioimmunotherapy in both univariate and multivariate analyses in some past studies but not in others (1,12,17–19). Only a univariate analysis was pursued in the present study because the nondosimetric factors did not show a statistically significant association with outcome whereas the dosimetric factors and equivalent biologic effect, which showed a statistically significant association with outcome, are strongly correlated with each other and hence cannot be used to develop multivariate models that simultaneously evaluate the effect of these factors.

The clear separation of PFS curves when stratified by a threshold tumor-absorbed dose of only 200 cGy may be surprising in the context of conventional external-beam radiotherapy, in which traditionally doses greater than 20 Gy are used for follicular and other indolent lymphomas. Although the relatively small number of patients in each group should be kept in mind when interpreting Figure 4, it is well known that follicular lymphoma is highly radiosensitive and high response rates with low-dose radiation have been reported previously (20–22). The cited studies report OR rates of approximately 85% after only 4 Gy in two 2-Gy fractions of involved-field radiotherapy in patients with low-grade, mostly follicular, lymphoma, which is similar to that for the greater-than-200-cGy group reported here (OR in 23/30 patients, or 77%). The mechanisms that drive the sensitivity of lymphomas to low-dose radiation are poorly understood. An explanation may be cellular response to radiation via early (or rapid) apoptosis in lymphoid cells (23). Apoptosis is one of the main cell death mechanisms in response to radiation. Lymphoid cells have been shown to die by apoptosis in both rapid and slow-dying cell lines (24). Early apoptosis occurs within hours of radiation exposure and does not require initiation by cell division. This process is highly radiation-sensitive and most often is p53-dependent. Delayed apoptosis occurs in association with G2/M arrest or as

a postmitotic event (mitotic catastrophe) and is likely less radio-sensitive (25).

Bone marrow dosimetry and the dose–toxicity correlation, which are also integral to radioimmunotherapy treatment planning, were not investigated in the present study. Accurate estimation of absorbed dose to the active (red) marrow is more difficult than tumor dosimetry because of the complex structure of the spongiosa and is beyond the scope of the present paper. We are developing methodology for accurate red marrow dosimetry based on SPECT/CT imaging of marrow-rich regions coupled with Monte Carlo–based computation of dose–rate to active marrow (26).

## CONCLUSION

The most important finding of the present study is the clearly demonstrated separation of PFS curves when stratified by mean tumor-absorbed dose. This result and the robust correlation shown between predicted and delivered tumor-absorbed doses demonstrate the potential for tumor dosimetry–driven treatment planning in radioimmunotherapy of NHL.

## DISCLOSURE

The costs of publication of this article were defrayed in part by the payment of page charges. Therefore, and solely to indicate this fact, this article is hereby marked “advertisement” in accordance with 18 USC section 1734. This work was supported by grant R01 EB001994 awarded by the National Institutes of Health, United States Department of Health and Human Services. Dr. Kaminski receives research support from GlaxoSmithKline and royalties from Bexxar. No other potential conflict of interest relevant to this article was reported.

## REFERENCES

- Jacene HA, Filice R, Kasecamp W, Wahl RL. Comparison of  $^{90}\text{Y}$ -ibritumomab tiuxetan and  $^{131}\text{I}$ -tositumomab in clinical practice. *J Nucl Med*. 2007;48:1767–1776.
- Kaminski MS, Tuck M, Estes J, et al.  $^{131}\text{I}$ -tositumomab therapy as initial treatment for follicular lymphoma. *N Engl J Med*. 2005;352:441–449.
- DeNardo GL, Denardo SJ, Balhorn R. Update: systemic radiotherapy can cure lymphoma—a paradigm for other malignancies? *Cancer Biother Radiopharm*. 2008;23:383–397.
- Sgouras G, Squeri S, Ballangrud AM, et al. Patient-specific, 3-dimensional dosimetry in non-Hodgkin’s lymphoma patients treated with  $^{131}\text{I}$ -anti-B1 antibody: assessment of tumor dose-response. *J Nucl Med*. 2003;44:260–268.
- Dewaraja YK, Schipper MJ, Roberson PL, et al.  $^{131}\text{I}$ -tositumomab radioimmunotherapy: initial tumor dose-response results using 3-dimensional dosimetry including radiobiologic modeling. *J Nucl Med*. 2010;51:1155–1162.
- Koral KF, Dewaraja Y, Li J, et al. Update on hybrid conjugate-view SPECT tumor dosimetry and response in  $^{131}\text{I}$ -tositumomab therapy of previously untreated lymphoma patients. *J Nucl Med*. 2003;44:457–464.
- Wilderman SJ, Dewaraja Y. Method for fast CT/SPECT-based 3D Monte Carlo absorbed dose computations in internal emitter therapy. *IEEE Trans Nucl Sci*. 2007;54:146–151.
- Dale RG. The application of the linear-quadratic dose-effect equation to fractionated and protracted radiotherapy. *Br J Radiol*. 1985;58:515–528.
- Roberson PL, Amro H, Wilderman SJ, et al. Bio-effect model applied to  $^{131}\text{I}$  radioimmunotherapy of refractory non-Hodgkin’s lymphoma. *Eur J Nucl Med Mol Imaging*. 2011;38:874–883.
- Cheng L, Hobbs RF, Segars PW, Sgouras G, Frey EC. Improved dose–volume histogram estimates for radiopharmaceutical therapy by optimizing quantitative SPECT reconstruction parameters. *Phys Med Biol*. 2013;58:3631–3647.
- Cheson BD, Pfister B, Juweid ME, et al. Revised response criteria for malignant lymphoma. *J Clin Oncol*. 2007;25:579–586.
- Fisher RI, Kaminski MS, Wahl RL, et al. Tositumomab and iodine-131 tositumomab produces durable complete remissions in a subset of heavily pretreated patients with low-grade and transformed non-Hodgkin’s lymphomas. *J Clin Oncol*. 2005;23:7565–7573.
- Schipper MJ, Koral KF, Avram AM, Kaminski MS, Dewaraja YK. Prediction of therapy tumor-absorbed dose estimates in  $^{131}\text{I}$  radioimmunotherapy using

- tracer data via a mixed-model fit to time activity. *Cancer Biother Radiopharm.* 2012;27:403–411.
14. Davis TA, Kaminski MS, Leonard JP, et al. The radioisotope contributes significantly to the activity of radioimmunotherapy. *Clin Cancer Res.* 2004;10:7792–7798.
  15. Dewaraja YK, Frey EC, Sgouros G, et al. MIRD pamphlet no. 23: quantitative SPECT for patient-specific 3-dimensional dosimetry in internal radionuclide therapy. *J Nucl Med.* 2012;53:1310–1325.
  16. Dewaraja Y, Avram AM, Roberson P, et al. Tumor absorbed dose predicts progression free survival (PFS) following I-131 radioimmunotherapy (RIT) [abstract]. *J Nucl Med.* 2013;54(suppl 2):16P.
  17. Vose JM, Wahl RL, Saleh M, et al. Multicenter phase II study of iodine-131 tositumomab for chemotherapy-relapsed/refractory low-grade and transformed low-grade B-cell non-Hodgkin's lymphomas. *J Clin Oncol.* 2000;18:1316–1323.
  18. Kaminski MS, Zelenetz AD, Press OW, et al. Pivotal study of iodine I 131 tositumomab for chemotherapy-refractory low-grade or transformed low-grade B-cell non-Hodgkin's lymphomas. *J Clin Oncol.* 2001;19:3918–3928.
  19. Kaminski MS, Estes J, Zasadny KR, et al. Radioimmunotherapy with iodine <sup>131</sup>I tositumomab for relapsed or refractory B-cell non-Hodgkin lymphoma: updated results and long-term follow-up of the University of Michigan experience. *Blood.* 2000;96:1259–1266.
  20. Girinsky T, Guillot-Vals D, Koscielny S, et al. A high and sustained response rate in refractory or relapsing low-grade lymphoma masses after low-dose radiation: analysis of predictive parameters of response to treatment. *Int J Radiat Oncol Biol Phys.* 2001;51:148–155.
  21. Haas RL, Poortmans P, De Jong D, et al. High response rates and lasting remissions after low-dose involved field radiotherapy in indolent lymphomas. *J Clin Oncol.* 2003;21:2474–2480.
  22. Murthy V, Thomas K, Foo K, et al. Efficacy of palliative low-dose involved-field radiation therapy in advanced lymphoma: a phase II study. *Clin Lymphoma Myeloma.* 2008;8:241–245.
  23. Radford IR. Radiation response of mouse lymphoid and myeloid cell lines. Part I. Sensitivity to killing by ionizing radiation, rate of loss of viability, and cell type of origin. *Int J Radiat Biol.* 1994;65:203–215.
  24. Radford IR, Murphy T, Radley J, Ellis S. Radiation response of mouse lymphoid and myeloid cell lines. Part II. Apoptotic death is shown by all lines examined. *Int J Radiat Biol.* 1994;65:217–227.
  25. Eriksson D, Riklund K, Johansson L, Strigbrand T. Radiation induced cell deaths. In: Stigbrand T, Carlsson J, Adams GP, eds. *Targeted Radionuclide Tumor Therapy: Biological Aspects.* Berlin, Germany: Springer; 2008:215–248.
  26. Wilderman SJ, Roberson P, Bolch W, Dewaraja Y. Investigation of effect of variations in bone fraction and red marrow cellularity on bone marrow dosimetry in radio-immunotherapy. *Phys Med Biol.* 2013;58:4717–4731.